JOURNAL OF GUIDANCE, CONTROL, AND DYNAMICS
Vol. 38, No. 5, May 2015

Engineering Notes

Controllability Analysis for Multirotor Helicopter Rotor Degradation and Failure

Guang-Xun Du,* Quan Quan,† Binxian Yang,‡ and Kai-Yuan Cai§
Beihang University, 100191 Beijing, People's Republic of China

DOI: 10.2514/1.G000731

Nomenclature

f_i	=	lift of ith rotor, N
g	=	acceleration of gravity, kg · m/s^2
h	=	altitude of helicopter, m
J_x, J_y, J_z	=	moment of inertia around roll, pitch, and yaw axes of helicopter frame, kg · m^2
K_i	=	maximum lift of ith rotor, N
k_μ	=	ratio between reactive torque and lift of rotors
L, M, N	=	airframe roll, pitch, and yaw torque of helicopter, N · m
m	=	number of rotors
m_a	=	mass of helicopter, kg
p, q, r	=	roll, pitch, and yaw angular velocities of helicopter, rad/s
r_i	=	distance from center of ith rotor to center of mass, m
T	=	total thrust of helicopter, N
v_h	=	vertical velocity of helicopter, m/s
η_i	=	efficiency parameter of ith rotor
ϕ, θ, ψ	=	roll, pitch, and yaw angles of helicopter, rad

I. Introduction

MULTIROTOR helicopters [1–3] are attracting increasing attention in recent years because of their important contribution and cost-effective application in several tasks, such as surveillance, search and rescue missions, and so on. However, there exists a potential risk to civil safety if a multirotor aircraft crashes, especially in an urban area. Therefore, it is of great importance to consider the flight safety of multirotor helicopters in the presence of rotor faults or failures [4].

Fault-tolerant control (FTC) [5] has the potential to improve the safety and reliability of multirotor helicopters. FTC is the ability of a controlled system to maintain or gracefully degrade control objectives despite the occurrence of a fault [6]. There are many applications in which fault tolerance may be achieved by using adaptive control, reliable control, or reconfigurable control strategies [7,8]. Some strategies involve explicit fault diagnosis and some do not. The reader is referred to a recent survey paper [9] for an outline of the state of the art in the field of FTC. However, only few attempts are known that focus on the fundamental FTC property analysis, one of which is defined as the (control) reconfigurability [6]. A faulty multirotor system with inadequate reconfigurability cannot be made to effectively tolerate faults, regardless of the feedback control strategy used [10]. The control reconfigurability can be analyzed from the intrinsic and performance-based perspectives. The aim of this Note is to analyze the control reconfigurability for multirotor systems (4-, 6-, and 8-rotor helicopters, etc.) from the controllability analysis point of view.

Classical controllability theories of linear systems are not sufficient to test the controllability of the considered multirotor helicopters because the rotors can only provide unidirectional lift (upward or downward) in practice. In our previous work [11], it was shown that a hexacopter with the standard symmetrical configuration is uncontrollable if one rotor fails, though the controllability matrix of the hexacopter is row full rank. Thus, the reconfigurability based on the controllability gramian [10] is no longer applicable. Brammer [12] proposed a necessary and sufficient condition for the controllability of linear autonomous systems with positive constraint, which can be used to analyze the controllability of multirotor systems. However, the theorems in [12] are not easy to use in practice. Owing to this, the controllability of a given system is reduced to those of its subsystems with real eigenvalues based on the Jordan canonical form in [13]. However, appropriate stable algorithms to compute Jordan real canonical form should be used to avoid ill-conditioned calculations. Moreover, a step-by-step controllability test procedure is not given. To address these problems, in this Note, the theory proposed in [12] is extended and a new necessary and sufficient condition of controllability is derived for the considered multirotor systems.

Nowadays, larger multirotor aircraft are starting to emerge and some multirotor aircraft are controlled by varying the collective pitch of the blade. This work considers only the multirotor helicopters controlled by varying the rpm of each rotor, but this research can be extended to most multirotor aircraft regardless of size, whether they are controlled by varying the collective pitch of the blade or the rpm.

The linear dynamic model of the considered multirotor helicopters around hover conditions is derived first, and then the control constraint is specified. It is pointed out that classical controllability theories of linear systems are not sufficient to test the controllability of the derived model (Sec. II). Then the controllability of the derived model is studied based on the theory in [12], and two conditions that are necessary and sufficient for the controllability of the derived model are given. To make the two conditions easy to test in practice, an Available Control Authority Index (ACAI) is introduced to quantify the available control authority of the considered multirotor systems. Based on the ACAI, a new necessary and sufficient condition is given to test the controllability of the considered multirotor systems (Sec. III). Furthermore, the computation of the proposed ACAI and a step-by-step controllability test procedure is approached for practical application (Sec. IV). The proposed controllability test method is used to analyze the controllability of a class of hexacopters to show its effectiveness (Sec. V). The major contributions of this Note are 1) an ACAI to quantify the available control authority of the considered multirotor systems, 2) a new necessary and sufficient controllability test condition based on the proposed ACAI, and 3) a step-by-step controllability test procedure for the considered multirotor systems.

Received 5 May 2014; revision received 27 October 2014; accepted for publication 6 November 2014; published online 20 January 2015.

*Ph.D. Candidate, School of Automation Science and Electrical Engineering; dgx@buaa.edu.cn.
†Associate Professor, School of Automation Science and Electrical Engineering; qq_buaa@buaa.edu.cn.
‡Graduate Student, School of Automation Science and Electrical Engineering; yangbinxian@asee.buaa.edu.cn.
§Professor, School of Automation Science and Electrical Engineering; kycai@buaa.edu.cn.

II. Problem Formulation

This Note considers a class of multirotor helicopters shown in Fig. 1, which are often used in practice. From Fig. 1, it can be seen that there are various types of multirotor helicopters with different rotor numbers and different configurations. Despite the difference in type and configuration, they can all be modeled in a general form as Eq. (1). In reality, the dynamic model of the multirotor helicopters is nonlinear and there is some aerodynamic damping and stiffness. However, if the multirotor helicopter is hovering, the aerodynamic damping and stiffness is ignorable. The linear dynamic model around hover conditions is given as [14–16]:

$$\dot{\boldsymbol{x}} = \boldsymbol{A}\boldsymbol{x} + \boldsymbol{B}\underbrace{(\boldsymbol{F} - \boldsymbol{G})}_{\boldsymbol{u}} \tag{1}$$

where

$$\begin{aligned}
&\boldsymbol{x} = [\,h \quad \phi \quad \theta \quad \psi \quad v_h \quad p \quad q \quad r\,]^T \in \mathbb{R}^8,\\
&\boldsymbol{F} = [\,T \quad L \quad M \quad N\,]^T \in \mathbb{R}^4,\\
&\boldsymbol{G} = [\,\boldsymbol{m_a g} \quad 0 \quad 0 \quad 0\,]^T \in \mathbb{R}^4,\\
&\boldsymbol{A} = \begin{bmatrix} \boldsymbol{0}_{4\times4} & \boldsymbol{I}_4 \\ \boldsymbol{0} & \boldsymbol{0} \end{bmatrix} \in \mathbb{R}^{8\times8},\\
&\boldsymbol{B} = \begin{bmatrix} \boldsymbol{0} \\ \boldsymbol{J}_f^{-1} \end{bmatrix} \in \mathbb{R}^{8\times4},\\
&\boldsymbol{J}_f = \mathrm{diag}(-m_a, J_x, J_y, J_z)
\end{aligned}$$

In practice, $f_i \in [0, K_i]$, $i = 1, \ldots, m$ because the rotors can only provide unidirectional lift (upward or downward). As a result, the rotor lift $\boldsymbol{f}$ is constrained by

$$\boldsymbol{f} \in \mathcal{F} = \Pi_{i=1}^{m}[0, K_i] \tag{2}$$

Then, according to the geometry of the multirotor system shown in Fig. 2, the mapping from the rotor lift f_i, $i = 1, \ldots, m$ to the system total thrust/torque $\boldsymbol{F}$ is

$$\boldsymbol{F} = \boldsymbol{B}_f \boldsymbol{f} \tag{3}$$

where $\boldsymbol{f} = [\,f_1 \quad \cdots \quad f_m\,]^T$. The matrix $\boldsymbol{B}_f \in \mathbb{R}^{4\times m}$ is the control effectiveness matrix and

$$\boldsymbol{B}_f = [\,\boldsymbol{b}_1 \quad \boldsymbol{b}_2 \quad \cdots \quad \boldsymbol{b}_m\,] \tag{4}$$

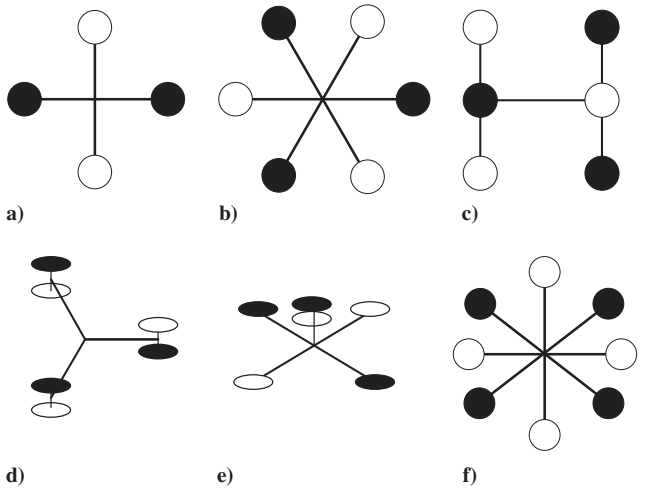

Fig. 1 Different configurations of multirotor helicopters: (white disk) rotor rotates clockwise; (black disk) rotor rotates counterclockwise.

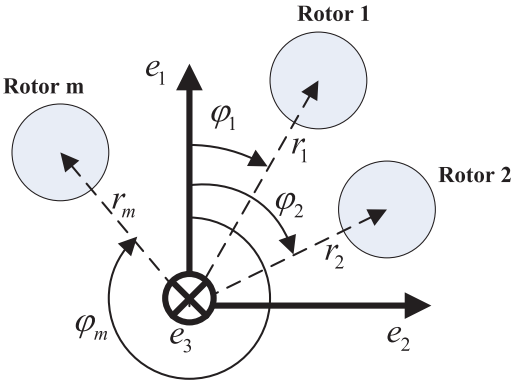

Fig. 2 Geometry definition for multirotor system.

where $\boldsymbol{b}_i = \eta_i \bar{\boldsymbol{b}}_i$, $\bar{\boldsymbol{b}}_i \in \mathbb{R}^4$, $i \in \{1, \ldots, m\}$ is the vector of contribution factors of the ith rotor to the total thrust/torque F; the parameters $\eta_i \in [0, 1]$, $i = 1, \ldots, 6$ is used to account for rotor wear/failure. If the ith rotor fails, then $\eta_i = 0$. For a multirotor helicopter whose geometry is shown in Fig. 2, the control effectiveness matrix $\boldsymbol{B}_f$ in parameterized form is [16]

$$\boldsymbol{B}_f = \begin{bmatrix} \eta_1 & \cdots & \eta_m \\ -\eta_1 r_1 \sin(\varphi_1) & \cdots & -\eta_m r_m \sin(\varphi_m) \\ \eta_1 r_1 \cos(\varphi_1) & \cdots & \eta_m r_m \cos(\varphi_m) \\ \eta_1 w_1 k_\mu & \cdots & \eta_m w_m k_\mu \end{bmatrix} \tag{5}$$

where w_i is defined by

$$w_i = \begin{cases} 1, & \text{if rotor } i \text{ rotates anticlockwise} \\ -1, & \text{if rotor } i \text{ rotates clockwise} \end{cases} \tag{6}$$

By Eqs. (2) and (3), $\boldsymbol{F}$ is constrained by

$$\Omega = \{\boldsymbol{F} | \boldsymbol{F} = \boldsymbol{B}_f \boldsymbol{f}, \boldsymbol{f} \in \mathcal{F}\} \tag{7}$$

Then, $\boldsymbol{u}$ is constrained by

$$\mathcal{U} = \{\boldsymbol{u} | \boldsymbol{u} = \boldsymbol{F} - \boldsymbol{G}, \boldsymbol{F} \in \Omega\} \tag{8}$$

From Eqs. (2), (7), and (8), $\mathcal{F}$, Ω, and $\mathcal{U}$ are all convex and closed.

Our major objective is to study the controllability of system (1) under the constraint $\mathcal{U}$.

Remark 1: The system (1) with constraint set $\mathcal{U} \subset \mathbb{R}^4$ is called controllable if, for each pair of points $\boldsymbol{x}_0 \in \mathbb{R}^8$ and $\boldsymbol{x}_1 \in \mathbb{R}^8$, there exists a bounded admissible control $\boldsymbol{u}(\boldsymbol{t}) \in \mathcal{U}$, defined on some finite interval $0 \le t \le t_1$, which steers $\boldsymbol{x}_0$ to $\boldsymbol{x}_1$. Specifically, the solution to system (1) $\boldsymbol{x}[t, \boldsymbol{u}(\cdot)]$ satisfies the boundary conditions $\boldsymbol{x}[0, \boldsymbol{u}(\cdot)] = \boldsymbol{x}_0$ and $\boldsymbol{x}[t_1, \boldsymbol{u}(\cdot)] = \boldsymbol{x}_1$.

Remark 2: Classical controllability theories of linear systems often require the origin to be an interior point of $\mathcal{U}$ so that $\boldsymbol{\mathcal{C}}(\boldsymbol{A}, \boldsymbol{B})$ being row full rank is a necessary and sufficient condition [12]. However, the origin is not always inside control constraint $\mathcal{U}$ of system (1) under rotor failures. Consequently, $\boldsymbol{\mathcal{C}}(\boldsymbol{A}, \boldsymbol{B})$ being row full rank is not sufficient to test the controllability of system (1).

III. Controllability for the Multirotor Systems

In this section, the controllability of system (1) is studied based on the positive controllability theory proposed in [12]. Applying the positive controllability theorem in [12] to system (1) directly, the following theorem is obtained:

Theorem 1: The following conditions are necessary and sufficient for the controllability of system (1):

1) Rank $\boldsymbol{\mathcal{C}}(\boldsymbol{A}, \boldsymbol{B}) = 8$, where $\boldsymbol{\mathcal{C}}(\boldsymbol{A}, \boldsymbol{B}) = [\,\boldsymbol{B} \quad \boldsymbol{AB} \quad \cdots \quad \boldsymbol{A}^7\boldsymbol{B}]$.

2) There is no real eigenvector $\boldsymbol{v}$ of A^T satisfying $\boldsymbol{v}^T\boldsymbol{Bu} \le 0$ for all $\boldsymbol{u} \in \mathcal{U}$.

It is difficult to test condition 2 in Theorem 1 because, in practice, one cannot check all $\boldsymbol{u}$ in $\mathcal{U}$. In the following, an easy-to-use criterion is proposed to test condition 2 in Theorem 1. Before going further, a measure is defined as

$$\rho(\boldsymbol{X}, \partial\Omega) \triangleq \begin{cases} \min\{\|\boldsymbol{X}-\boldsymbol{F}\|:\ \boldsymbol{X}\in\Omega, \boldsymbol{F}\in\partial\Omega\} \\ -\min\{\|\boldsymbol{X}-\boldsymbol{F}\|:\ \boldsymbol{X}\in\Omega^C, \boldsymbol{F}\in\partial\Omega\} \end{cases} \tag{9}$$

where $\partial\Omega$ is the boundary of Ω, and Ω^C is the complementary set of Ω. If $\rho(\boldsymbol{X}, \partial\Omega) \le 0$, then $\boldsymbol{X} \in \Omega^C \cup \partial\Omega$, which means that $\boldsymbol{X}$ is not an interior point of Ω. Otherwise, $\boldsymbol{X}$ is an interior point of Ω.

According to Eq. (9), $\rho(\boldsymbol{G}, \partial\Omega) = \min\{\|\boldsymbol{G}-\boldsymbol{F}\|, \boldsymbol{F}\in\partial\Omega\}$, which is the radius of the biggest enclosed sphere centered at $\boldsymbol{G}$ in the attainable control set Ω. In practice, it is the maximum control thrust/torque that can be produced in all directions. Therefore, it is an important quantity to ensure controllability for arbitrary rotor wear/failure. Then, $\rho(\boldsymbol{G}, \partial\Omega)$ can be used to quantify the available control authority of system (1). From Eq. (8), it can be seen that all the elements in $\mathcal{U}$ are given by translating the all the elements in Ω by a constant $\boldsymbol{G}$. Because translation does not change the relative position of all the elements of Ω, the value of $\rho(\boldsymbol{0}, \partial\mathcal{U})$ is equal to the value of $\rho(\boldsymbol{G}, \partial\Omega)$. In this Note, the ACAI of system (1) is defined by $\rho(\boldsymbol{G}, \partial\Omega)$ because Ω is the attainable control set and more intuitive than $\mathcal{U}$ in practice. The ACAI shows the ability as well as the control capacity of a multirotor helicopter controlling its altitude and attitude. With this definition, the following lemma about condition 2 of Theorem 1 is obtained.

Lemma 1: The following three statements are equivalent for system (1):

1) There is no nonzero real eigenvector $\boldsymbol{v}$ of $\boldsymbol{A}^T$ satisfying $\boldsymbol{v}^T\boldsymbol{B}\boldsymbol{u} \le 0$ for all $\boldsymbol{u}\in\mathcal{U}$ or $\boldsymbol{v}^T\boldsymbol{B}(\boldsymbol{F}-\boldsymbol{G}) \le 0$ for all $\boldsymbol{F}\in\Omega$.

2) $\boldsymbol{G}$ is an interior point of Ω.

3) The ACAI $\rho(\boldsymbol{G}, \partial\Omega) > 0$.

Proof: See Appendix A. □

By Lemma 1, condition 2 in Theorem 1 can be tested by the value $\rho(\boldsymbol{G}, \partial\Omega)$. Now, a new necessary and sufficient condition can be derived to test the controllability of system (1).

Theorem 2: System (1) is controllable, if and only if the following two conditions hold: 1) rank $\mathcal{C}(\boldsymbol{A}, \boldsymbol{B}) = 8$; 2) $\rho(\boldsymbol{G}, \partial\Omega) > 0$.

According to Lemma 1, Theorem 2 is straightforward from Theorem 1. Actually, Theorem 2 is a corollary of Theorem 1.4 presented in [12]. To make this Note more readable and self-contained, we extend the condition (1.6) of Theorem 1.4 presented in [12], and get condition 2 in Theorem 2 of this Note based on the simplified structure of the $(\boldsymbol{A}, \boldsymbol{B})$ pair and the convexity of $\mathcal{U}$. This extension can enable the quantification of the controllability and also make it possible to develop a step-by-step controllability test procedure for the multirotor systems. In the following section, a step-by-step controllability test procedure is approached based on Theorem 2.

IV. Step-by-Step Controllability Test Procedure

This section will show how to obtain the value of the proposed ACAI in Sec. III. Furthermore, a step-by-step controllability test procedure for the controllability of system (1) is approached for practical applications.

A. Available Control Authority Index Computation

First, two index matrices $\boldsymbol{S}_1$ and $\boldsymbol{S}_2$ are defined, where $\boldsymbol{S}_1$ is a matrix whose rows consist of all possible combinations of three elements of $\boldsymbol{M} = [\,1 \quad 2 \quad \cdots \quad m\,]$, and the corresponding rows of $\boldsymbol{S}_2$ are the remaining $m-3$ elements of $\boldsymbol{M}$. The matrix $\boldsymbol{S}_1$ contains s_m rows and three columns, and the matrix $\boldsymbol{S}_2$ contains s_m rows and $m-3$ columns, where

$$s_m = \frac{m!}{(m-(n_\Omega-1))!(n_\Omega-1)!} \tag{10}$$

For the system in Eq. (1), s_m is the number of the groups of parallel boundary segments in $\mathcal{F}$. For example, if $m=4$, $n_\Omega=4$, then $s_m = 4$ and

$$\boldsymbol{S}_1 = \begin{bmatrix} 1 & 2 & 3 \\ 1 & 2 & 4 \\ 1 & 3 & 4 \\ 2 & 3 & 4 \end{bmatrix}, \qquad \boldsymbol{S}_2 = \begin{bmatrix} 4 \\ 3 \\ 2 \\ 1 \end{bmatrix}$$

Define $\boldsymbol{B}_{1,j}$ and $\boldsymbol{B}_{2,j}$ as follows:

$$\begin{aligned} \boldsymbol{B}_{1,j} &= [\,\boldsymbol{b}_{S_1(j,1)} \quad \boldsymbol{b}_{S_1(j,2)} \quad \boldsymbol{b}_{S_1(j,3)}\,] \in \mathbb{R}^{4\times 3} \\ \boldsymbol{B}_{2,j} &= [\,\boldsymbol{b}_{S_2(j,1)} \quad \cdots \quad \boldsymbol{b}_{S_2(j,m-3)}\,] \in \mathbb{R}^{4\times(m-3)} \end{aligned} \tag{11}$$

where $j = 1, \ldots, s_m$, $\boldsymbol{S}_1(j,k_1)$ is the element at the jth row and the k_1th column of $\boldsymbol{S}_1$, and $\boldsymbol{S}_2(j,k_2)$ is the element at the jth row and the k_2th column of $\boldsymbol{S}_2$. Here $k_1 = 1, 2, 3$ and $k_2 = 1, \ldots, m-3$.

Define a sign function sign$(\cdot)$ as follows: for an n-dimensional vector $\boldsymbol{a} = [\,a_1 \quad \ldots \quad a_n\,] \in \mathbb{R}^{1\times n}$,

$$\text{sign}(\boldsymbol{a}) = [\,c_1 \quad \cdots \quad c_n\,] \tag{12}$$

where $c_i = 1$ if $a_i > 0$, $c_i = 0$ if $a_i = 0$, and $c_i = -1$ if $a_i < 0$. Then, $\rho(\boldsymbol{G}, \partial\Omega)$ is obtained by the following theorem.

Theorem 3: For the system in Eq. (1), if rank $\boldsymbol{B}_f = 4$, then the ACAI $\rho(\boldsymbol{G}, \partial\Omega)$ is given by

$$\rho(G, \partial\Omega) = \text{sign}(\min(d_1, d_2, \ldots, d_{s_m}))\min(|d_1|, |d_2|, \ldots, |d_{s_m}|) \tag{13}$$

If rank $\boldsymbol{B}_{1,j} = 3$, then

$$\begin{aligned} d_j = \frac{1}{2}\text{sign}(\boldsymbol{\xi}_j^T\boldsymbol{B}_{2,j})\boldsymbol{\Lambda}_j(\boldsymbol{\xi}_j^T\boldsymbol{B}_{2,j})^T - |\boldsymbol{\xi}_j^T(\boldsymbol{B}_f\boldsymbol{f}_c - \boldsymbol{G})|, \\ j = 1, \ldots, s_m \end{aligned} \tag{14}$$

where $\boldsymbol{f}_c = \frac{1}{2}[\,K_1 \quad K_2 \quad \cdots \quad K_m\,]^T \in \mathbb{R}^m$ and $\boldsymbol{\Lambda}_j \in \mathbb{R}^{(m-3)\times(m-3)}$ is given by

$$\boldsymbol{\Lambda}_j = \begin{bmatrix} K_{S_2(j,1)} & 0 & 0 & 0 \\ 0 & K_{S_2(j,2)} & 0 & 0 \\ & & \ddots & \\ 0 & 0 & 0 & K_{S_2(j,m-3)} \end{bmatrix} \tag{15}$$

The vector $\boldsymbol{\xi}_j \in \mathbb{R}^4$ satisfies

$$\boldsymbol{\xi}_j^T\boldsymbol{B}_{1,j} = 0, \qquad \|\boldsymbol{\xi}_j\| = 1 \tag{16}$$

and $\boldsymbol{B}_{1,j}$ and $\boldsymbol{B}_{2,j}$ are given by Eq. (11). If rank $\boldsymbol{B}_{1,j} < 3$, $d_j = +\infty$.

Proof: The proof process is divided into three steps and the details can be found in Appendix B. □

Remark 3: In practice, $+\infty$ is replaced by a sufficiently large positive number (for example, set $d_j = 10^6$). If rank $\boldsymbol{B}_f < 4$, then Ω is not a four-dimensional hypercube and the ACAI makes no sense, which is set to $-\infty$. (Similarly, $-\infty$ is replaced by -10^6 in practice.) From Eq. (13), if $\rho(\boldsymbol{G}, \partial\Omega) > 0$, then $\boldsymbol{G}$ is an interior point of Ω and $\rho(\boldsymbol{G}, \partial\Omega)$ is the minimum distance from $\boldsymbol{G}$ to $\partial\Omega$. If $\rho(\boldsymbol{G}, \partial\Omega) < 0$, then $\boldsymbol{G}$ is not an interior point of Ω and $|\rho(\boldsymbol{G}, \partial\Omega)|$ is the minimum distance from $\boldsymbol{G}$ to $\partial\Omega$. The ACAI $\rho(\boldsymbol{G}, \partial\Omega)$ can also be used to show a degree of controllability (see [17–19]) of the system in Eq. (1), but the ACAI is fundamentally different from the degree of controllability in [17]. The degree of controllability in [17] is defined based on the minimum Euclidean norm of the state on the boundary of the recovery region for time t. However, the ACAI is defined based on the minimum Euclidean norm of the control force on the boundary of the attainable control set. The degree of controllability in [17] is time dependent, whereas the ACAI is time independent. A very

similar multirotor failure assessment was provided in [16] by computing the radius of the biggest circle that fits in the L-M plane with the center in the origin ($L = 0, M = 0$), where the L-M plane is obtained by cutting the four-dimensional attainable control set at the nominal hovering conditions defined with $T = \boldsymbol{m}_a \boldsymbol{g}$ and $N = 0$. This computation is very simple and intuitive. However, the radius of the two-dimensional L-M plane can only quantify the control authority of roll and pitch control. To account for this, the ACAI proposed by this Note is defined by the radius of the biggest ball that fits in the four-dimensional polytopes Ω with the center in $\boldsymbol{G}$.

B. Controllability Test Procedure for Multirotor Systems

From the preceding, the controllability of the multirotor system (1) can be analyzed by the following procedure:

Step 1) Check the rank of $\mathcal{C}(\boldsymbol{A}, \boldsymbol{B})$. If $\mathcal{C}(\boldsymbol{A}, \boldsymbol{B}) = 8$, go to step 2. If $\mathcal{C}(\boldsymbol{A}, \boldsymbol{B}) < 8$, go to step 9.

Step 2) Set the value of the rotor's efficiency parameter η_i, $i = 1, \ldots, m$ to get $\boldsymbol{B}_f = [\,\boldsymbol{b}_1 \quad \boldsymbol{b}_2 \quad \cdots \quad \boldsymbol{b}_m\,]$ as shown in Eq. (4). If rank $\boldsymbol{B}_f = 4$, go to step 3. If rank $\boldsymbol{B}_f < 4$, let $\rho(\boldsymbol{G}, \partial\Omega) = -10^6$ and go to step 9.

Step 3) Compute the two index matrices $\boldsymbol{S}_1$ and $\boldsymbol{S}_2$, where $\boldsymbol{S}_1$ is a matrix whose rows consist of all possible combinations of the m elements of $\boldsymbol{M}$ taken three at a time, and the rows of S_2 are the remaining $(m-3)$ elements of $\boldsymbol{M}$, $\boldsymbol{M} = [\,1 \quad 2 \quad \cdots \quad m\,]$.

Step 4) Let $j = 1$.

Step 5) Compute the two matrices $\boldsymbol{B}_{1,j}$ and $\boldsymbol{B}_{2,j}$ according to Eq. (11).

Step 6) If rank $\boldsymbol{B}_{1,j} = 3$, compute d_j according to Eq. (14). If rank $\boldsymbol{B}_{1,j} < 3$, set $d_j = 10^6$.

Step 7) Let $j = j + 1$. If $j \le s_m$, go to step 5. If $j > s_m$, go to step 8.

Step 8) Compute $\rho(\boldsymbol{G}, \partial\Omega)$ according to Eq. (13).

Step 9) If $\mathcal{C}(\boldsymbol{A}, \boldsymbol{B}) < 8$ or $\rho(\boldsymbol{G}, \partial\Omega) \le 0$, system (1) is uncontrollable. Otherwise, the system in Eq. (1) is controllable.

V. Controllability Analysis for a Class of Hexacopters

In this section, the controllability test procedure developed in Sec. IV is used to analyze the controllability of a class of hexacopters shown in Fig. 3, subject to rotor wear/failures, to show its effectiveness. The rotor arrangement of the considered hexacopter is the standard symmetrical configuration shown in Fig. 3a. PNPNPN is used to denote the standard arrangement, where "P" denotes that a rotor rotates clockwise and "N" denotes that a rotor rotates counterclockwise. According to Eq. (4), the control effectiveness matrix $\boldsymbol{B}_f$ of that hexacopter configuration is

$$\boldsymbol{B}_f = \begin{bmatrix} \eta_1 & \eta_2 & \eta_3 & \eta_4 & \eta_5 & \eta_6 \\ 0 & -\frac{\sqrt{3}}{2}\eta_2 r_2 & -\frac{\sqrt{3}}{2}\eta_3 r_3 & 0 & \frac{\sqrt{3}}{2}\eta_5 r_5 & \frac{\sqrt{3}}{2}\eta_6 r_6 \\ \eta_1 r_1 & \frac{1}{2}\eta_2 r_2 & -\frac{1}{2}\eta_3 r_3 & -\eta_4 r_4 & -\frac{1}{2}\eta_5 r_5 & \frac{1}{2}\eta_6 r_6 \\ -\eta_1 k_\mu & \eta_2 k_\mu & -\eta_3 k_\mu & \eta_4 k_\mu & -\eta_5 k_\mu & \eta_6 k_\mu \end{bmatrix} \tag{17}$$

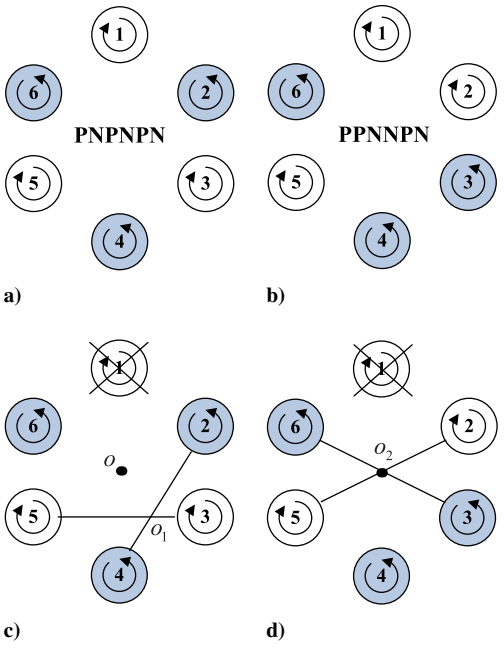

Fig. 3 Depiction of a) standard and b) new rotor arrangement, and first rotor of c) PNPNPN and d) PPNNPN system fails.

Table 1 Hexacopter parameters

Parameter	Value	Units
m_a	1.535	kg
g	9.80	m/s^2
r_i, $i = 1, \ldots, 6$	0.275	m
K_i, $i = 1, \ldots, 6$	6.125	N
J_x	0.0411	kg · m^2
J_y	0.0478	kg · m^2
J_z	0.0599	kg · m^2
k_μ	0.1	— —

Table 2 Hexacopter (PNPNPN) controllability with one rotor failed

Rotor failure	Rank of $\mathcal{C}(\boldsymbol{A}, \boldsymbol{B})$	ACAI	Controllability
No wear/failure	8	1.4861	Controllable
$\eta_1 = 0$	8	0	Uncontrollable
$\eta_2 = 0$	8	0	Uncontrollable
$\eta_3 = 0$	8	0	Uncontrollable
$\eta_4 = 0$	8	0	Uncontrollable
$\eta_5 = 0$	8	0	Uncontrollable
$\eta_6 = 0$	8	0	Uncontrollable

Table 3 Hexacopter (PPNNPN) controllability with one rotor failed

Rotor failure	Rank of $\mathcal{C}(\boldsymbol{A}, \boldsymbol{B})$	ACAI	Controllability
No wear/failure	8	1.1295	Controllable
$\eta_1 = 0$	8	0.7221	Controllable
$\eta_2 = 0$	8	0.4510	Controllable
$\eta_3 = 0$	8	0.4510	Controllable
$\eta_4 = 0$	8	0.7221	Controllable
$\eta_5 = 0$	8	0	Uncontrollable
$\eta_6 = 0$	8	0	Uncontrollable

The physical parameters of the prototype hexacopter are shown in Table 1. Using the procedure defined in Sec. IV, the controllability analysis results of the PNPNPN hexacopter subject to one rotor failure is shown in Table 2. The PNPNPN hexacopter is uncontrollable when one rotor fails, even though its controllability matrix is row full rank. A new rotor arrangement (PPNNPN) of the hexacopter shown in Fig. 3b is proposed in [16], which is still controllable when one of some specific rotors stops. The controllability of the PPNNPN hexacopter subject to one rotor failure is shown in Table 3.

From Tables 2 and 3, the value of the ACAI is 1.4861 for the PNPNPN hexacopter, subject to no rotor failures, whereas the value of the ACAI is reduced to 1.1295 for the PPNNPN hexacopter. It can be observed that the use of the PPNNPN configuration instead of the PNPNPN configuration improves the fault-tolerance capabilities but also decreases the ACAI for the no-failure condition. Similar to the results in [16], changing the rotor arrangement is always a tradeoff between fault tolerance and control authority. That said, the PPNNPN system is not always controllable under a failure. From Table 3, it can be seen that, if the fifth or sixth rotor fails, the PPNNPN system is uncontrollable.

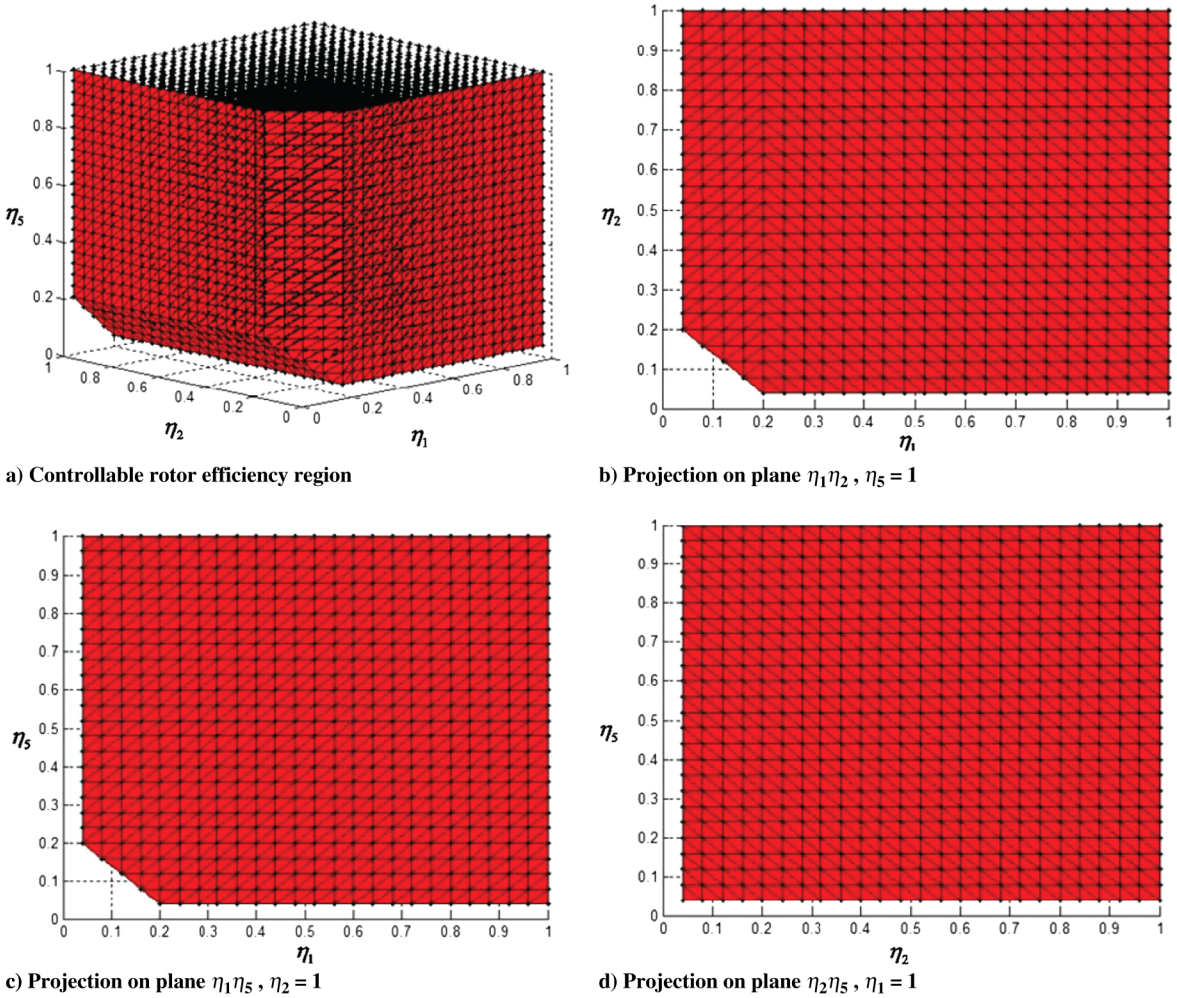

a) Controllable rotor efficiency region

b) Projection on plane $\eta_1\eta_2$, $\eta_5 = 1$

c) Projection on plane $\eta_1\eta_5$, $\eta_2 = 1$

d) Projection on plane $\eta_2\eta_5$, $\eta_1 = 1$

Fig. 4 Controllable region of different rotors' efficiency parameter for PNPNPN hexacopter.

The following provides some physical insight between the two configurations. For the PPNNPN configuration, if one of the rotors (other than the fifth and sixth rotor) of that system fails, the remaining rotors still comprise a basic quadrotor configuration that is symmetric about the mass center (see Fig. 3d). In contrast, if one rotor of the PNPNPN system fails, although the remaining rotors can make up a basic quadrotor configuration, the quadrotor configuration is not symmetric about the mass center (see Fig. 3c). The result is that the PPNNPN system under most single rotor failures can provide the necessary thrust and torque control, whereas the PNPNPN system cannot.

Therefore, it is necessary to test the controllability of the multirotor helicopters before any fault-tolerant control strategies are employed. Moreover, the controllability test procedure approached can also be used to test the controllability of the hexacopter with different η_i, $i \in \{1, \ldots, 6\}$. Let η_1, η_2, and η_5 vary in $[0, 1] \subset \mathbb{R}$, namely, rotors 1, 2, and 5 are worn; then the PNPNPN hexacopter retains controllability while η_1, η_2, and η_5 are in the grid region (where the grid spacing is 0.04) in Fig. 4. The corresponding ACAI at the boundaries of the projections shown in Fig. 4 is zero or near to zero (because of error in numerical calculation).

VI. Conclusions

The controllability problem of a class of multirotor helicopters was investigated. An ACAI was introduced to quantify the available control authority of multirotor systems. Based on the ACAI, a new necessary and sufficient condition was given based on a positive controllability theory. Moreover, a step-by-step procedure was developed to test the controllability of the considered multirotor helicopters. The proposed controllability test method was used to analyze the controllability of a class of hexacopters to show its effectiveness. Analysis results showed that the hexacopters with different rotor configurations have different fault tolerant capabilities. It is therefore necessary to test the controllability of the multirotor helicopters before any fault-tolerant control strategies are employed.

Appendix A: Proof of Lemma 1

To make this Note self-contained, the following Lemma is introduced.

Lemma 3 [20]: If Ω is a nonempty convex set in $\mathbb{R}^4$ and $\boldsymbol{F}_0$ is not an interior point of Ω, then there is a nonzero vector $\boldsymbol{k}$ such that $\boldsymbol{k}^T(\boldsymbol{F} - \boldsymbol{F}_0) \leq 0$ for each $\boldsymbol{F} \in \mathrm{cl}(\Omega)$, where $\mathrm{cl}(\Omega)$ is the closure of Ω.

Then, according to Lemma 3,

$1 \Rightarrow 2$): Suppose that condition 1 holds. It is easy to see that all the eigenvalues of $\boldsymbol{A}^T$ are zero. By solving the linear equation $\boldsymbol{A}^T\boldsymbol{v} = 0$, all the eigenvectors of $\boldsymbol{A}^T$ are expressed in the following form:

$$\boldsymbol{v} = [0 \quad 0 \quad 0 \quad 0 \quad k_1 \quad k_2 \quad k_3 \quad k_4]^T \tag{A1}$$

where $\boldsymbol{v} \neq 0$, $\boldsymbol{k} = [k_1 \quad k_2 \quad k_3 \quad k_4]^T \in \mathbb{R}^4$, and $\boldsymbol{k} \neq 0$. With it,

$$\boldsymbol{v}^T\boldsymbol{B}\boldsymbol{u} = -k_1\frac{T - m_a g}{m_a} + k_2\frac{L}{J_x} + k_3\frac{M}{J_y} + k_4\frac{N}{J_z} \tag{A2}$$

By Lemma 3, if $\boldsymbol{G}$ is not an interior point of Ω, then $\boldsymbol{u} = \boldsymbol{0}$ is not an interior point of $\mathcal{U}$. Then, there is a nonzero $\boldsymbol{k}_u = [k_{u1} \quad k_{u2} \quad k_{u3} \quad k_{u3}]^T$ satisfying

$$\boldsymbol{k}_u^T\boldsymbol{u} = k_{u1}(T - m_a g) + k_{u2}L + k_{u3}M + k_{u4}N \leq 0$$

for all $\boldsymbol{u} \in \mathcal{U}$. Let

$$\boldsymbol{k} = [\,-k_{u1}m_a \quad k_{u2}J_x \quad k_{u3}J_y \quad k_{u4}J_z\,]^T \tag{A3}$$

then, $\boldsymbol{v}^T\boldsymbol{B}\boldsymbol{u} \le 0$ for all $\boldsymbol{u} \in \mathcal{U}$ according to Eq. (A2), which contradicts Theorem 1.

$2 \Rightarrow 1$): Because all the eigenvectors of $\boldsymbol{A}^T$ are expressed in the form expressed by Eq. (A1), then

$$\boldsymbol{v}^T\boldsymbol{B}\boldsymbol{u} = \boldsymbol{k}^T\boldsymbol{J}_f^{-1}\boldsymbol{u}$$

according to Eqs. (1) and (A1), where $\boldsymbol{k} \neq 0$. Then, the statement that there is no nonzero $\boldsymbol{v} \in \mathbb{R}^8$ expressed by Eq. (A1) satisfying $\boldsymbol{v}^T\boldsymbol{B}\boldsymbol{u} \le 0$ for all $\boldsymbol{u} \in \mathcal{U}$ is equivalent to that there is no nonzero $\boldsymbol{k} \in \mathbb{R}^4$ satisfying $\boldsymbol{k}^T\boldsymbol{J}_f^{-1}\boldsymbol{u} \le 0$ for all $\boldsymbol{u} \in \mathcal{U}$. Supposing that condition 2 is valid, then $\boldsymbol{u} = 0$ is an interior point of $\mathcal{U}$. There is a neighborhood $\mathcal{B}(0, u_r)$ of $\boldsymbol{u} = 0$ belonging to $\mathcal{U}$, where $u_r > 0$ is small and constant. Condition $2 \Rightarrow 1$ will be proved by counterexamples.

Supposing that condition 1 does not hold, then there is a $\boldsymbol{k} \neq 0$ satisfying $\boldsymbol{k}^T\boldsymbol{J}_f^{-1}\boldsymbol{u} \le 0$ for all $\boldsymbol{u} \in \mathcal{U}$. Without loss of generality, let $\boldsymbol{k} = [\,k_1 \quad * \quad * \quad *\,]^T$ where $k_1 \neq 0$ and $*$ indicates an arbitrary real number. Let $\boldsymbol{u}_1 = [\,\varepsilon \quad 0 \quad 0 \quad 0\,]^T$ and $\boldsymbol{u}_2 = [\,-\varepsilon \quad 0 \quad 0 \quad 0\,]^T$ where $\varepsilon > 0$; then, $\boldsymbol{u}_1, \boldsymbol{u}_2 \in \mathcal{B}(0, u_r)$ if ε is sufficiently small. Because $\boldsymbol{k}^T\boldsymbol{J}_f^{-1}\boldsymbol{u} \le 0$ for all $\boldsymbol{u} \in \mathcal{B}(0, u_r)$, then $\boldsymbol{k}^T\boldsymbol{J}_f^{-1}\boldsymbol{u}_1 \le 0$ and $\boldsymbol{k}^T\boldsymbol{J}_f^{-1}\boldsymbol{u}_2 \le 0$. According to Eq. (1),

$$-\frac{k_1\varepsilon}{m_a} \le 0, \qquad \frac{k_1\varepsilon}{m_a} \le 0$$

This implies that $k_1 = 0$, which contradicts the fact that $k_1 \neq 0$. Then, condition 1 holds.

$2 \Leftrightarrow 3$): According to the definition of $\rho(\boldsymbol{G}, \partial\Omega)$, if $\rho(\boldsymbol{G}, \partial\Omega) \le 0$, then $\boldsymbol{G}$ is not in the interior of Ω, and if $\rho(\boldsymbol{G}, \partial\Omega) > 0$, then $\boldsymbol{G}$ is an interior point of Ω.

This completes the proof.

Appendix B: Proof of Theorem 3

Theorem 3 will be proved in the following three steps.

Step 1: Obtain Eq. (B5), which are the projection of parallel boundaries in $\mathcal{F}$ by the map $\boldsymbol{B}_f$.

The results in [17] are referenced to complete this step. First, Eq. (3) is rearranged as follows:

$$\boldsymbol{F} = [\,\boldsymbol{B}_{1,j} \quad \boldsymbol{B}_{2,j}\,]\begin{bmatrix}\boldsymbol{f}_{1,j}\\ \boldsymbol{f}_{2,j}\end{bmatrix} \tag{B1}$$

where $\boldsymbol{f}_{1,j} = [\,f_{S_1(j,1)} \quad f_{S_1(j,2)} \quad f_{S_1(j,3)}\,]^T \in \mathbb{R}^3$, $\boldsymbol{f}_{2,j} = [\,f_{S_2(j,1)} \quad \cdots \quad f_{S_2(j,m-3)}\,]^T \in \mathbb{R}^{m-3}$, $j = 1, \ldots, s_m$. Write Eq. (B1) more simply as

$$\boldsymbol{F} = \boldsymbol{B}_{1,j}\boldsymbol{f}_{1,j} + \boldsymbol{B}_{2,j}\boldsymbol{f}_{2,j} \tag{B2}$$

If the rank of $\boldsymbol{B}_{1,j}$ is three, there exists a four-dimensional vector $\boldsymbol{\xi}_j$ such that

$$\boldsymbol{\xi}_j^T\boldsymbol{B}_{1,j} = 0, \qquad \|\boldsymbol{\xi}_j\| = 1$$

Therefore, multiplying $\boldsymbol{\xi}_j^T$ on both sides of Eq. (B2) results in

$$\boldsymbol{\xi}_j^T\boldsymbol{F} - \boldsymbol{\xi}_j^T\boldsymbol{B}_{2,j}\boldsymbol{f}_{2,j} = 0 \tag{B3}$$

According to [17], $\partial\Omega$ is a set of hyperplane segments, and each hyperplane segment in $\partial\Omega$ is the projection of a three-dimensional boundary hyperplane segment of $\mathcal{F}$. Each three-dimensional boundary of the hypercube $\mathcal{F}$ can be characterized by fixing the values of $\boldsymbol{f}_{2,j}$ at the boundary value, denoted by $\bar{\boldsymbol{f}}_{2,j}$, where

$$\bar{\boldsymbol{f}}_{2,j} \in \Pi_{i=1}^{m-3}\{0, K_{S_2(j,i)}\} \tag{B4}$$

and allowing the values of $\boldsymbol{f}_{1,j}$ to vary between their limits given by $\mathcal{F}$, where $\boldsymbol{f}_{1,j} \in \Pi_{i=1}^{3}[0, K_{S_1(j,i)}]$. Then, for each j, if rank $\boldsymbol{B}_{1,j} = 3$, a group of parallel hyperplane segments $\Gamma_{\Omega,j} = \{l_{\Omega,j,k}, k = 1, \ldots, 2^{m-3}\}$ in Ω is obtained, and each $l_{\Omega,j,k}$ is expressed by

$$l_{\Omega,j,k} = \{\boldsymbol{X} | \boldsymbol{\xi}_j^T\boldsymbol{X} - \boldsymbol{\xi}_j^T\boldsymbol{B}_{2,j}\bar{\boldsymbol{f}}_{2,j} = 0, \boldsymbol{X} \in \Omega, \bar{\boldsymbol{f}}_{2,j} \in \Pi_{i=1}^{m-3}\{0, K_{S_2(j,i)}\}\} \tag{B5}$$

where $\boldsymbol{\xi}_j$ is the normal vector of the hyperplane segments.

Step 2: Compute the distances from the center $\boldsymbol{F}_c$ to all the elements of $\partial\Omega$.

It is pointed out that not all the hyperplane segments in $\Gamma_{\Omega,j}$ specified by Eq. (B5) belong to $\partial\Omega$. In fact, for each j, only two hyperplane segments specified by Eq. (B5) belong to $\partial\Omega$, denoted by $\Gamma_{\Omega,j,1}$ and $\Gamma_{\Omega,j,2}$, $j \in \{1, \ldots, s_m\}$, which are symmetric about the center $\boldsymbol{F}_c$ of Ω. The center of $\mathcal{F}$ is $\boldsymbol{f}_c$, then $\boldsymbol{F}_c$ is the projection of $\boldsymbol{f}_c$ through the map $\boldsymbol{B}_f$ and is expressed as follows:

$$\boldsymbol{F}_c = \boldsymbol{B}_f\boldsymbol{f}_c \tag{B6}$$

where $\boldsymbol{f}_c = \frac{1}{2}[\,K_1 \quad K_2 \quad \cdots \quad K_m\,]^T \in \mathbb{R}^m$. Then, the distances from $\boldsymbol{F}_c$ to the hyperplane segments given by Eq. (B5) are computed by

$$d_{\Omega,j,k} = |\boldsymbol{\xi}_j^T\boldsymbol{F}_c - \boldsymbol{\xi}_j^T\boldsymbol{B}_{2,j}\bar{\boldsymbol{f}}_{2,j}| = |\boldsymbol{\xi}_j^T\boldsymbol{B}_{2,j}(\bar{\boldsymbol{f}}_{2,j} - \boldsymbol{f}_{c,2})| = |\boldsymbol{\xi}_j^T\boldsymbol{B}_{2,j}\bar{\boldsymbol{z}}_j| \tag{B7}$$

where $k = 1, \ldots, 2^{m-3}$, $\boldsymbol{f}_{c,2} = \frac{1}{2}[K_{S_2(j,1)}K_{S_2(j,2)} \cdots K_{S_2(j,m-3)}]^T \in \mathbb{R}^{m-3}$, $\bar{\boldsymbol{f}}_{2,j}$ is specified by Eq. (B4), and $\bar{\boldsymbol{z}}_j = \bar{\boldsymbol{f}}_{2,j} - \boldsymbol{f}_{c,2}$.

Remark 4: The distances from $\boldsymbol{F}_c$ to the hyperplane segments given by Eq. (B5) are defined by $d_{\Omega,j,k} = \min\{\|\boldsymbol{X} - \boldsymbol{F}_c\|, \boldsymbol{X} \in l_{\Omega,j,k}\}$, $k = 1, \ldots, 2^{m-3}$.

The distances from the center $\boldsymbol{F}_c$ to $\Gamma_{\Omega,j,1}$ and $\Gamma_{\Omega,j,2}$ are equal, which is given by

$$d_{j,\max} = \max\{d_{\Omega,j,k}, k = 1, \ldots, 2^{m-3}\} \tag{B8}$$

Since

$$\bar{\boldsymbol{z}}_j \in Z = \frac{1}{2}\Pi_{i=1}^{m-3}\{-K_{S_2(j,i)}, K_{S_2(j,i)}\}, \qquad k = 1, \ldots, 2^{m-3}$$

$$d_{j,\max} = \frac{1}{2}\operatorname{sign}(\boldsymbol{\xi}_j^T\boldsymbol{B}_{2,j})\Lambda_j(\boldsymbol{\xi}_j^T\boldsymbol{B}_{2,j})^T \tag{B9}$$

according to Eqs. (12), (B7), and (B8), where $\boldsymbol{\Lambda}_j$ is given by Eq. (15).

Step 3: Compute $\rho(G, \partial\Omega)$.

Because $\boldsymbol{G}$ and $\boldsymbol{F}_c$ are known, the vector $\boldsymbol{F}_{Gc} = \boldsymbol{F}_c - \boldsymbol{G}$ is projected along the direction $\boldsymbol{\xi}_j$ and the projection is given by

$$d_{Gc} = \boldsymbol{\xi}_j^T\boldsymbol{F}_{Gc} \tag{B10}$$

Then, if $\boldsymbol{G} \in \Omega$, the minimum of the distances from $\boldsymbol{G}$ to both $\Gamma_{\Omega,j,1}$ and $\Gamma_{\Omega,j,2}$ is

$$d_j = d_{j,\max} - |d_{Gc}| \tag{B11}$$

However, if $\boldsymbol{G} \in \Omega^C$, d_j specified by Eq. (B11) may be negative. So the minimum of the distances from $\boldsymbol{G}$ to both $\Gamma_{\Omega,j,1}$ and $\Gamma_{\Omega,j,2}$ is $|d_j|$. According to Eqs. (B6) and (B9–B11),

$$d_j = \frac{1}{2}\operatorname{sign}(\boldsymbol{\xi}_j^T\boldsymbol{B}_{2,j})\boldsymbol{\Lambda}_j(\boldsymbol{\xi}_j^T\boldsymbol{B}_{2,j})^T - |\boldsymbol{\xi}_j^T(\boldsymbol{B}_f\boldsymbol{f}_c - \boldsymbol{G})|,$$

$$j = 1, \ldots, s_m$$

However, if rank $\boldsymbol{B}_{1,j} < 3$, the three-dimensional hyperplane segments are planes, lines, or points in $\partial\Omega$ or Ω and $|d_j|$ will never be the minimum in $|d_1|, |d_2|, \ldots, |d_{s_m}|$. The distance d_j is set to $+\infty$ if rank $\boldsymbol{B}_{1,j} < 3$. The purpose of this is to exclude d_j from

$|d_1|, |d_2|, \ldots, |d_{s_m}|$. In practice, $+\infty$ is replaced by a sufficiently large positive number (for example, $d_j = 10^6$). If $\min(d_1, d_2, \ldots, d_{s_m}) \geq 0$, then $\boldsymbol{G} \in \Omega$ and $\rho(\boldsymbol{G}, \partial\Omega) = \min(d_1, d_2, \ldots, d_{s_m})$. But if $\min(d_1, d_2, \ldots, d_{s_m}) < 0$, which implies that at least one of $d_j < 0$, $j \in \{1, \ldots, s_m\}$, then $\boldsymbol{G} \in \Omega^C$ and $\rho(\boldsymbol{G}, \partial\Omega) = -\min(|d_1|, |d_2|, \ldots, |d_{s_m}|)$ according to Eq. (9).

Then, $\rho(\boldsymbol{G}, \partial\Omega)$ is computed by

$$\rho(\boldsymbol{G}, \partial\Omega) = \text{sign}(\min(d_1, d_2, \ldots, d_{s_m}))\min(|d_1|, |d_2|, \ldots, |d_{s_m}|) \tag{B12}$$

This is consistent with the definition in Eq. (9).

Acknowledgments

This work is supported by the National Natural Science Foundation of China (61473012) and the "Young Elite" of High Schools in Beijing City of China (YETP1071).

References

[1] Mahony, R., Kumar, V., and Corke, P., "Multirotor Aerial Vehicles: Modeling Estimation and Control of Quadrotor," *IEEE Robotics & Automation Magazine*, Vol. 19, No. 3, 2012, pp. 20–32. doi:10.1109/MRA.2012.2206474

[2] Omari, S., Hua, M.-H., Ducard, G., and Hamel, T., "Hardware and Software Architecture for Nonlinear Control of Multirotor Helicopters," *IEEE/ASM Transactions on Mechatronics*, Vol. 18, No. 6, 2013, pp. 1724–1736. doi:10.1109/TMECH.2013.2274558

[3] Crowther, B., Lanzon, A., Maya-Gonzalez, M., and Langkamp, D., "Kinematic Analysis and Control Design for a Nonplanar Multirotor Vehicle," *Journal of Guidance, Control, and Dynamics*, Vol. 34, No. 4, 2011, pp. 1157–1171. doi:10.2514/1.51186

[4] Sadeghzadeh, I., Mehta, A., and Zhang, Y., "Fault/Damage Tolerant Control of a Quadrotor Helicopter UAV Using Model Reference Adaptive Control and Gain-Scheduled PID," *AIAA Guidance, Navigation, and Control Conference*, AIAA Paper 2011-6716, Aug. 2011, doi:10.2514/6.2011-6716

[5] Pachter, M., and Huang, Y.-S., "Fault Tolerant Flight Control," *Journal of Guidance, Control, and Dynamics*, Vol. 26, No. 1, 2003, pp. 151–160. doi:10.2514/2.5026

[6] Yang, Z., "Reconfigurability Analysis for a Class of Linear Hybrid Systems," *Proceedings of Sixth IFAC SAFEPRO-CESS'06*, Elsevier, New York, 2007, pp. 974–979. doi:10.1016/B978-008044485-7/50164-0

[7] Zhang, Y., and Jiang, J., "Integrated Design of Reconfigurable Fault-Tolerant Control Systems," *Journal of Guidance, Control, and Dynamics*, Vol. 24, No. 1, 2001, pp. 133–136. doi:10.2514/2.4687

[8] Cieslak, J., Henry, D., Zolghadri, A., and Goupil, P., "Development of an Active Fault-Tolerant Flight Control Strategy," *Journal of Guidance, Control, and Dynamics*, Vol. 31, No. 1, 2008, pp. 135–147. doi:10.2514/1.30551

[9] Zhang, Y., and Jiang, J., "Bibliographical Review on Reconfigurable Fault-Tolerant Control Systems," *Annual Reviews in Control*, Vol. 32, No. 2, 2008, pp. 229–252. doi:10.1016/j.arcontrol.2008.03.008

[10] Wu, N. E., Zhou, K., and Salomon, G., "Control Reconfigurability of Linear Time-Invariant Systems," *Automatica*, Vol. 36, No. 11, 2000, pp. 1767–1771. doi:10.1016/S0005-1098(00)00080-7

[11] Du, G.-X., Quan, Q., and Cai, K.-Y., "Controllability Analysis and Degraded Control for a Class of Hexacopters Subject to Rotor Failures," *Journal of Intelligent & Robotic Systems* [online], Sept. 2014. doi:10.1007/s10846-014-0103-0

[12] Brammer, R. F., "Controllability in Linear Autonomous Systems with Positive Controllers," *SIAM Journal on Control*, Vol. 10, No. 2, 1972, pp. 339–353. doi:10.1137/0310026

[13] Yoshida, H., and Tanaka, T., "Positive Controllability Test for Continuous-Time Linear Systems," *IEEE Transactions on Automatic Control*, Vol. 52, No. 9, 2007, pp. 1685–1689. doi:10.1109/TAC.2007.904278

[14] Ducard, G., and Hua, M-D., "Discussion and Practical Aspects on Control Allocation for a Multi-Rotor Helicopter," *Proceedings of the 1st International Conference on UAVs in Geomatics*, UAV-g-2011, Copernicus Publ., Göttingen, Germany, Sept. 2011, pp. 95–100.

[15] Du, G.-X., Quan, Q., and Cai, K.-Y., "Additive-State-Decomposition-Based Dynamic Inversion Stabilized Control of a Hexacopter Subject to Unknown Propeller Damages," *Proceedings of the 32nd Chinese Control Conference*, IEEE Computer Soc. Press, Piscataway, NJ, July 2013, pp. 6231–6236.

[16] Schneider, T., Ducard, G., Rudin, K., and Strupler, P., "Fault-Tolerant Multirotor Systems," Master Dissertation, ETH Zurich, Zurich, Switzerland, 2011.

[17] Klein, G., Lindberg, R. E., and Longman, R. W., "Computation of a Degree of Controllability via System Discretization," *Journal of Guidance, Control, and Dynamics*, Vol. 5, No. 6, 1982, pp. 583–588. doi:10.2514/3.19793

[18] Viswanathan, C. N., Longman, R. W., and Likins, P. W., "Degree of Controllability Definition: Fundamental Concepts and Application to Modal Systems," *Journal of Guidance, Control, and Dynamics*, Vol. 7, No. 2, 1984, pp. 222–230. doi:10.2514/3.8570

[19] Kang, O., Park, Y., Park, Y. S., and Suh, M., "New Measure Representing Degree of Controllability for Disturbance Rejection," *Journal of Guidance, Control, and Dynamics*, Vol. 32, No. 5, 2009, pp. 1658–1661. doi:10.2514/1.43864

[20] Goodwin, G., Seron, M., and Doná, J., "Overview of Optimisation Theory," *Constrained Control and Estimation: An Optimisation Approach*, 1st ed., Springer–Verlag, London, 2005, p. 31.